VNU Journal of Science: Mathematics – Physics, Vol. 41, No. 2 (2025) 92-106

VNU Journal of Science: Mathematics - Physics

Journal homepage: https://js.vnu.edu.vn/MaP

Original Article

Influence of Fabrication Conditions on the Magnetic Properties of $MnFe_2O_4$ Nanoparticles Synthesized by Hydrothermal Method

Nguyen Duy Xuan, Dao Xuan Trung Hieu, Le Duy Cuong, Ho Thi Anh*

VNU University of Engineering and Technology, 144 Xuan Thuy, Cau Giay, Hanoi, Vietnam

Received 28th March 2025
Revised 14th May 2025; Accepted 28th May 2025

Abstract: Manganese ferrite ($MnFe_2O_4$) nanoparticles have attracted significant research interest due to their unique magnetic properties and diverse applications in high-frequency devices, biomedical systems, and environmental treatment. In this work, we systematically investigated the influence of reaction times (T_r = 1–5 h) and pH values (4–13) on the crystallinity, morphology, and magnetic properties of $MnFe_2O_4$ nanoparticles synthesized by hydrothermal method at 150 °C. The samples characterization was carried-out by XRD, Fe-SEM, and VSM measurements. The experimental results demonstrated that optimal conditions were achieved at a pH value of 11 with T_r = 4 h, producing like-spherical nanoparticles with an average size of 25 nm. However, due to some agglomeration, the overall particle size distribution ranged from 15 to 60 nm, with an average size in non-aggregated regions around 40 nm. These nanoparticles exhibited outstanding magnetic properties, including a high saturation magnetization of ~ 57 emu/g, a low coercivity of ~ 22 Oe, and an experimental magnetic moment value of about 2.35 μ_B. In contrast, lower pH values or varying reaction times led to impurities and reduced magnetic performance. Additionally, the effects of annealing temperatures (200 – 800 °C) on the magnetic properties were explored. These results provide crucial insights into the synthesis-structure-property relationships in $MnFe_2O_4$ nanoparticles and establish practical guidelines for producing high-quality $MnFe_2O_4$ nanoparticles for applications in various fields.

Keywords: Manganese ferrite, hydrothermal, nanomaterials, magnetic properties.

* Corresponding author.
E-mail address: anhht@vnu.edu.vn

https//doi.org/10.25073/2588-1124/vnumap.4998

1. Introduction

Nanostructured materials have attracted significant attention in materials science research and applications over the past decade due to their remarkable mechanical, physical, chemical, and optical properties, which are enhanced at the nanoscale [1, 2]. These unique properties have opened up promising applications in diverse fields such as electronics, energy, biomedical sciences, and environmental engineering [1-4]. The term "spinel group" or "spinel crystal structures" originates from $MgAl_2O_4$, a non-magnetic mineral with a complex face-centered cubic structure found in nature [5]. Spinel ferrites share chemical composition and structural similarities with the spinel group, characterized by the general formula MFe_2O_4, where M represents a divalent metal such as Mn, Ni, Co, Zn, Cu, or a mixture [2]. Alternatively, M can be divalent iron, forming the magnetite (Fe_3O_4) material. Their face-centered cubic (fcc) structure influences the electronic and magnetic properties, with the distribution of metal ions at tetrahedral and octahedral sites significantly influencing the material's magnetic behavior [6-9]. The metal ions M can occupy either tetrahedral or octahedral positions, resulting in the formation of inverse spinel, normal spinel, and mixed spinel configurations. The characteristic properties of spinel ferrites, including electronic, magnetic, and optical behaviour, depending on the relative sizes of the cations, their charge, and the crystal field stabilization arising from the arrangement of octahedral and tetrahedral voids within the lattice [1, 2, 10, 11].

Manganese ferrite ($MnFe_2O_4$) is a prominent magnetic metal oxide nanoparticle studied for its properties such as low coercivity, high permeability, low loss, moderate saturation magnetization, and ease of magnetization and demagnetization [2, 3]. Consequently, this material has become the focus of extensive research, with applications in high-frequency antenna devices [12, 13], radar signal absorption coatings [14], biomedical materials [15, 16], and contrast enhancement in MRI [17]. The magnetic and optical properties of spinel ferrites are generally influenced by crystalline size, morphology, impurities, and the distribution of cations at tetrahedral and octahedral sites [18]. In the case of $MnFe_2O_4$, its mixed spinel structure is primarily determined by the dominance of the Fe^{3+} (tetra) - Fe^{3+} (octa) exchange interaction over the Mn^{2+} (tetra) - Fe^{3+} (octa) interaction. Different synthesis methods can lead to the partial oxidation of Mn^{2+} to Mn^{3+} ions, which have a magnetic moment of 4 μ_B/f.u, compared to Fe^{3+} ions that have a magnetic moment of 5 μ_B/f.u. [19]. These Mn^{3+} ions preferentially occupy octahedral sites, which increases the inversion degree and decreases the magnetization. Achieving a low inversion degree, which is crucial for enhancing magnetization, remains an experimental challenge for scientists and is strongly correlated with the synthesis approach and the oxidation state of manganese ions [20, 21].

The fabrication method strongly influences the properties of $MnFe_2O_4$, and recent research has focused on different fabrication methods and the characterization of $MnFe_2O_4$ nanoparticles. Studies have shown that the magnetic properties of Mn ferrite are sensitive to particle size, which can be controlled by varying synthesis conditions such as pH, temperature, and reaction time. Various synthesis methods, including solvothermal [22], sol-gel [23], co-precipitation [24], polyol [25], microwave-induced combustion [26], and hydrothermal [27-29], have been explored. Each method has its advantages and disadvantages, and researchers select the appropriate synthesis method based on available laboratory equipment and specific research goals. Among these methods, the hydrothermal process stands out due to its ability to precisely control particle size and ensure uniform distribution. Additionally, its versatility, simplicity, and low cost have made it a popular choice for nanoparticle fabrication. Despite its popularity, systematic investigations into the effects of key experimental parameters, such as pH and reaction time, on the structural and magnetic properties of $MnFe_2O_4$ are still limited.

This work systematically explored the hydrothermal synthesis of $MnFe_2O_4$ nanoparticles under varying fabrication conditions to understand their direct impact on the structure and magnetic properties. The reaction time ranged from 1 to 5 h, and the pH values varied from 4 to 13. Additionally, the

optimized sample was subjected to annealing at temperatures between 200 and 800 °C to investigate the effect of annealing temperature on the magnetic properties. The results of this study provide valuable insights into the synthesis-structure-property relationships in $MnFe_2O_4$ nanoparticles and offer critical guidance for tailoring their magnetic properties. These findings pave the way for the potential application of $MnFe_2O_4$ nanoparticles in advanced magnetic devices, including high-frequency technologies, biomedical systems, and environmental remediation.

2. Experimental

2.1. Materials

The chemicals used to synthesize $MnFe_2O_4$ nanomaterials were of analytical grade including: Iron (III) nitrate nonahydrate ($Fe(NO_3)_3.9H_2O$, ≥98.5%, AR-Xinglong), manganese (II) chloride tetrahydrate ($MnCl_2.4H_2O$, ≥99.0%, AR-Xinglong), potassium hydroxide (KOH, ≥ 85.0%, AR-Xinglong), deionized water (DI) and used without further purification.

2.2. Synthesis of $MnFe_2O_4$ Nanoparticles

The manganese ferrite ($MnFe_2O_4$) nanoparticles were prepared using a facile hydrothermal method. Firstly, 20 mmol $Fe(NO_3)_3.9H_2O$ and 10 mmol $MnCl_2.4H_2O$ (ratio Mn^{2+}: Fe^{3+} = 1:2) were dissolved in 40 ml DI water by magnetic stirring. After 15 minutes, 4M KOH solution was added drop-wise to the mixture over 20 minutes to adjust the pH to the desired value while continuing to stir. The mixed solution was then transferred into a Teflon-lined stainless-steel autoclave with a 100 mL capacity. Initially, to optimize the reaction time, samples were prepared at pH13, synthesis temperature of 150 °C, with different holding times (samples labeled as T1 to T5 corresponding to reaction times of 1, 2, 3, 4, and 5 h, respectively). After determining that 4 h was the optimal reaction time, the effect of pH was investigated by preparing samples at different pH values while maintaining the reaction time of 4 h at 150 °C (samples labeled as P1, P2, P3, P4, and P5 corresponding to pH values of 4, 7, 9, 11, and 13, respectively). After the hydrothermal process, the solid precipitate was collected by washing with DI water and centrifugation at 5000 rpm for 20 minutes, repeated three times. The collected material was then dried in a vacuum oven at 80 °C for 8 h. The dried $MnFe_2O_4$ powder was ground by an agate mortar and pestle for 1 hour to form a fine powder.

2.3. Characterization

The structural parameters of $MnFe_2O_4$ powder were characterized by X-ray diffraction on the XRD EQUINOX 5000 device (CuK_α, λ = 0.0154 nm, 2θ steps = 0.03 θ/step). Field emission scanning electron microscopy (Fe-SEM) is used to study the morphology and average size of nanoparticles. Using a vibrating sample magnetometer on the Lakeshore 7404 device (5 – 10 kOe, room temperature) to investigate the magnetic properties of the fabricated samples. The optimal sample was annealed at 200 °C, 400 °C, 600 °C, and 800 °C for 4 h in air using a Nabertherm RT 50/250/13 tube furnace.

3. Results and Discussions

3.1. X-ray Diffraction (XRD) Analysis

Figure 1 presents the XRD patterns of ten $MnFe_2O_4$ samples synthesized under different experimental parameters. The synthesis conditions significantly affect the phase compositions of the samples. The XRD patterns reveal two crystalline phases: α-Fe_2O_3 (marked by an asterisk) and $MnFe_2O_4$. Based on the relative intensities of the diffraction peaks, samples synthesized at high pH values (P3 – P5) and with longer hydrothermal reaction times (T3 – T5) exhibit better crystallinity. These patterns display diffraction peaks corresponding to the spinel structure and match the standard JCPDS card number 88-1965 [30]. The observed peaks at 29.03°, 35.18°, 35.40°, 43.18°, 53.57°, 56.20°, and 62.57° correspond to the (220), (222), (311), (400), (442), (511), and (440) planes, respectively. Among these, the (311) peak shows the highest intensity, indicating the dominant cubic spinel phase. In contrast, samples P1, P2, T1, and T2 contained noticeable impurity phases, particularly α-Fe_2O_3, as indicated by JCPDS card number 79-000 [31].

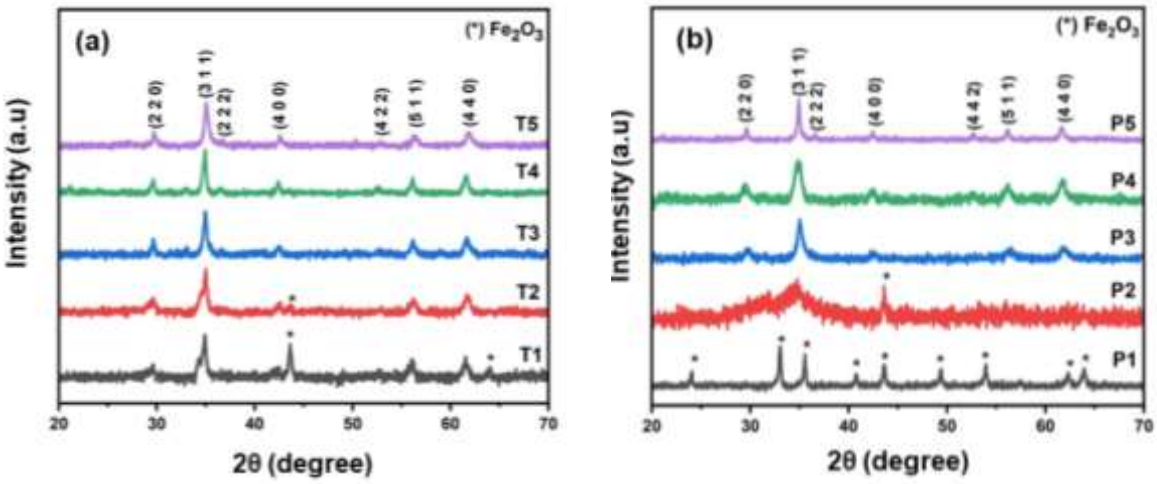

Figure 1. X-ray diffraction of $MnFe_2O_4$ nanoparticles prepared at different reaction time (a) and different pH (b).

We found that the main diffraction peak (311) of samples T1 and T2 exhibited peak splitting, with the appearance of secondary peaks, the intensity of impurity peaks gradually decreased with increasing reaction time. Sample P2 display quasi-amorphous characteristics in its XRD pattern, showing broad and poorly defined peaks with low intensity, accompanied by significant background noise. Additionally, one impurity peak (marked in the figure) was observed, indicating the presence of a secondary phase. This reflects poor crystallinity and incomplete phase formation. When the reaction time is not long enough, the formation and growth of $MnFe_2O_4$ particles are not complete, potentially leading to the presence of intermediate phases or impurities, the spinel structure is not completely formed, and the crystals have defects. While at low pH, the OH^- concentration in the solution is not enough to promote the complete precipitation reaction of Mn^{2+} and Fe^{3+} ions, leading to the formation of α-Fe_2O_3 sub-phase instead of pure $MnFe_2O_4$. Therefore, it can be concluded that the combination of higher pH and longer reaction time will increase the reaction efficiency, which is the decisive factor to achieve well-crystalline $MnFe_2O_4$ with minimal impurities.

These results are in line with previous studies using the hydrothermal method for the synthesis of $MnFe_2O_4$ nanoparticles. For instance, Kwon et al. [27] synthesized $MnFe_2O_4$ nanoparticles using a hydrothermal method at 140 °C, which also showed the formation of $MnFe_2O_4$ with a cubic spinel structure. The study found that increasing the reaction temperature led to improved crystallinity and reduced impurity phases, similar to our observations. Their results revealed that at higher reaction temperatures (160 – 200 °C), the $MnFe_2O_4$ phase dominated, with sharper peaks and reduced Fe_2O_3

contamination, indicating a higher degree of crystallinity. In addition, Tombuloglu et al. [28] also synthesized $MnFe_2O_4$ nanoparticles using the hydrothermal method at 220 °C and pH10, and their XRD results showed that the $MnFe_2O_4$ nanoparticles were a fine crystalline structure with no detectable impurity phases. This suggests that the reaction conditions used in their study led to the formation of $MnFe_2O_4$ nanoparticles, similar to what we have observed in our study. These studies support our findings that optimizing the synthesis conditions, particularly for pH and reaction time, is crucial to achieving high-quality $MnFe_2O_4$ nanoparticles.

The crystallite size of the samples was determined using the maximum intensity peak (311) by Scherrer's equation [31]:

$$D = \frac{k.\lambda}{\beta.\cos\theta} \quad (1)$$

where k represents the Scherrer constant, λ is the wavelength of the X-ray radiation, β denotes the full width at half maximum (FWHM) of the peak, and θ is the Bragg diffraction angle. An increase in reaction time leads to a gradual increase in the average size of the crystal, while the largest pH results in the largest size of the crystallity.

Since the structure of this ferrite is spinel cubic, the lattice constant is determined using the following relation [32]:

$$\frac{1}{d^2} = \frac{h^2+k^2+l^2}{a^2} \quad (2)$$

Where d is the inter-planar distance, (hkl) are the Miller indices, and a is the lattice constant. $MnFe_2O_4$ nanoparticles are produced by the hydrothermal method with lattice parameters ranging from 10.8 to 24.3 nm.

To calculate the unit cell volume, the lattice parameter a is used according to the formula:

$$V = a^3 \quad (3)$$

Table 1 demonstrates the structural parameters like volume, crystallite size of samples P3 – P5 and T1 – T5. Various structural parameters, like crystallite size, lattice constant, are demonstrated in Table 1.

Adjusting the hydrothermal reaction time alters the lattice parameters of the samples, as shown in Fig. 1 and confirmed in Table 1, leading to shifts in the peaks observed in the XRD patterns. Specifically, for reaction times increasing from 1 to 5 h at pH13, the average crystal size increased from 11.26 nm (T1) to 21.21 nm (T4), indicating improved crystallinity with longer reaction times. However, when the reaction time was extended to 5 h (T5), the crystal size decreased to 15.64 nm. Thus, a reaction time of 4 h was identified as optimal for achieving the best crystallinity and particle size.

Table 1. Structural parameters of samples P3 – P5 and T1 – T5

Sample	Peak position (^{o})	FWHM (^{o})	D (nm)	Lattice Constant (Å)	Volume (nm^3)
T1	34.77	0.77	11.26	0.8519	0.6183
T2	34.87	0.75	11.54	0.8496	0.6133
T3	34.93	0.47	18.28	0.8515	0.6174
T4	34.88	0.41	21.21	0.8517	0.6178
T5	35.06	0.55	15.64	0.8484	0.6107
P3	35.07	0.73	11.82	0.8489	0.6117
P4	34.86	0.80	10.80	0.8550	0.6250
P5	34.93	0.35	24.30	0.8512	0.6167

Upon determining the optimal reaction time, additional samples were synthesized at varying pH levels to evaluate the influence of pH on the crystal structure. As the pH increased, the crystallinity improved, and the particle size gradually increased from 11.82 nm (P3) at pH = 9 to 24.3 nm (P5) at pH = 13. These results indicate that higher pH values are more favorable for the formation of well-crystallized $MnFe_2O_4$ nanoparticles, further supporting the role of pH in controlling particle growth during hydrothermal synthesis. The findings from our study suggest that the optimal combination of lower temperature and shorter reaction time in our approach can significantly reduce energy consumption while maintaining the desired quality of $MnFe_2O_4$ nanoparticles.

3.2. Fe-SEM Analysis

The morphology and particle size of $MnFe_2O_4$ materials synthesized under different reaction times were examined using Fe-SEM images. The Fe-SEM images of T3 and T4 are presented in Fig. 2a, b taken at 500 nm scale. In the T3 sample, a significant presence of large agglomerates is observed, which could be attributed to the grinding process during the experiment. As Zhang et al. [33] pointed out, the large surface area of the nanoparticles leads to strong electrostatic attraction and van der Waals forces between them, causing the particles to easily aggregate into larger clusters. Moreover, as Akash Solunke et al. [34] emphasized, when the pH is not properly controlled (especially when pH is far from the optimal value, such as near pH7), the reaction may not proceed fully, leading to incomplete reaction and the formation of agglomerated particles. This incomplete reaction can hinder proper densification of the nanoparticles, further contributing to the agglomeration. Despite the aggregation into large clusters, the nanoparticles surrounding these agglomerates were measured to be approximately 30 to 40 nm in size. This result is notably larger than the particle size values obtained from XRD measurements. The average crystallite size calculated from the XRD pattern using the Scherrer formula typically reflects the size of the particles within the measured region, which is usually smaller than the size observed in SEM images, as the Scherrer formula measures the internal size of the particle and does not account for the deformation of the outer shell.

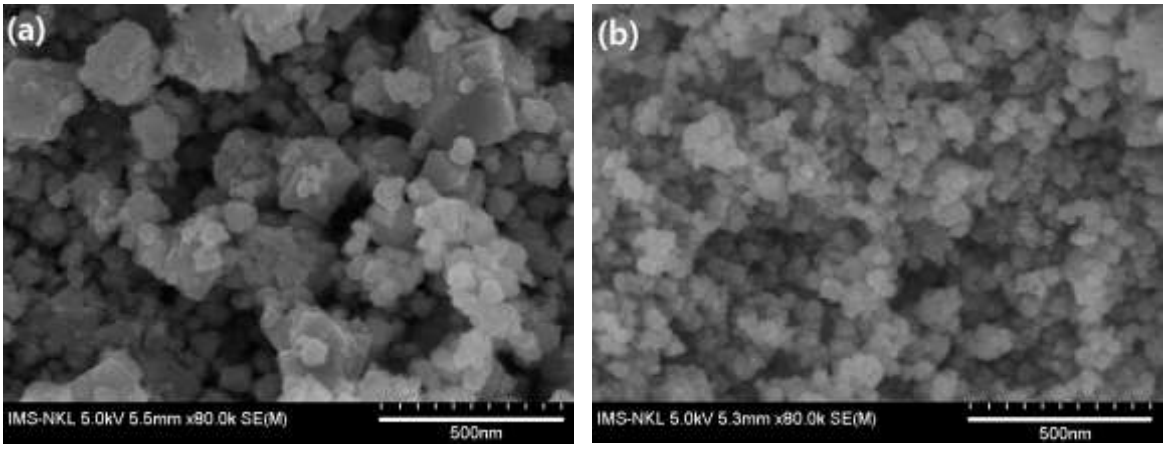

Figure 2. Fe-SEM image of $MnFe_2O_4$ nanoparticles fabricated at T= 150 ^oC, pH = 11 with different time (a) T3 and (b) T4.

Conversely, when the reaction time increased, sample T4 showed a nearly uniform distribution of aggregated nanoparticles with minimal agglomeration, and the particle size of this sample was

approximately 25 nm. Consequently, it can be concluded that increasing the reaction time improves the nanoparticle size, resulting in smaller and more uniformly distributed particles.

Figure 3 shows the P4 sample synthesized with a reaction time of 4 h at pH11, captured at two scales: 300 nm (a) and 500 nm (b). The $MnFe_2O_4$ nanoparticles formed are all spherical in shape, with highly crystallized nanoparticles exhibiting a wide size distribution. The grain size of P4 was primarily found to be around 25 nm, though due to some aggregation, the size distribution extends from 15 to 60 nm, with an average of approximately 40 nm in non-agglomerated regions.

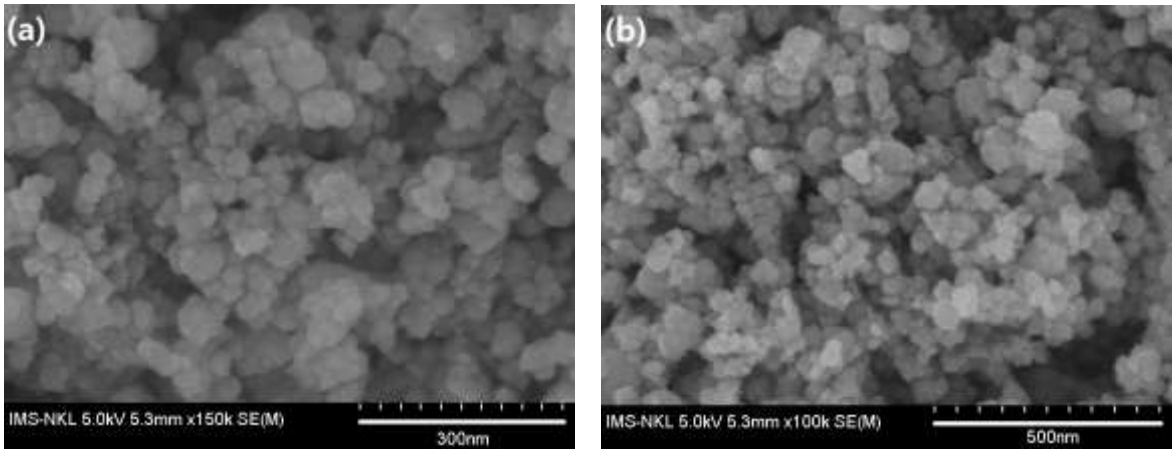

Figure 3. Fe-SEM image of $MnFe_2O_4$ nanoparticles at P4 value (pH = 11) taken at scale (a). 300 nm and (b). 500 nm.

In hydrothermal synthesis, the pH of the precursor solution plays a critical role in determining the chelation behavior of metal ions and the nucleation–growth kinetics of nanoparticles. Although our system is hydrothermal, the underlying principle is consistent with previous findings using sol–gel methods, according to Solunke et al. [34], where varying the pH alters the degree of metal ion chelation, affecting chemical reactions and combustion behavior during nanoparticle formation. Additionally, changes in pH affect the reaction rate, which in turn influences nanoparticle growth, as explained in detail by Ghahfarokhi et al. [5]. Therefore, adjusting the pH during the hydrothermal process can significantly influence the size, shape, and crystallinity of the resulting nanoparticles, which in turn impacts their structural and magnetic properties.

Fe-SEM showed that the high pH value and long-time reaction favor the growth of highly crystalline nanoparticles and uniform particle size distribution. Although there is a variation in size compared to the XRD results, the crystallization trend is entirely consistent with the data from XRD.

3.3. Magnetic Measurements

The magnetic properties of the samples are characterized by the M-H hysteresis loop obtained by the vibrating sample magnetometer (VSM) technique at room temperature and demonstrated in Figures 4 and 5. Tables 2 and 3 show the values such as saturation magnetization (M_s), remanent magnetization (M_r), and coercivity (H_c) determined from the hysteresis loop.

Figure 4 illustrates the M-H loops of the $MnFe_2O_4$ samples at different reaction times. It can be seen that all M-H loops exhibit S-shapes with small areas, high M_s values, low H_c, and clear magnetic saturation at elevated fields. Thereby, demonstrating the soft ferromagnetic behavior of the prepared nanoparticles. From Fig. 4 and Table 2, it is possible to see that sample T4 has the highest magnetism. As the reaction time increased, the saturation magnetization gradually increased from 35.76 emu/g

(sample T1) to 53.4 emu/g (sample T4) and then decreased to 46.93 emu/g (sample T5), following a non-linear trend. This behavior confirms that the hydrothermal reaction time significantly influences the crystallinity and magnetic properties of $MnFe_2O_4$, consistent with the trend in previously reported spinel ferrites [35-37]. However, when the reaction time is prolonged, the average crystallite size of the sample (T5) decreases to 15.64 nm, which is smaller than that of T4 (21.21 nm). This reduction in size may partly contribute to the decline in Ms, as smaller crystallites can weaken magnetic exchange interactions, a trend also observed in Fe_3O_4 nanoparticles as reported by Sneha Upadhyay et al. [38]. In addition, extended hydrothermal duration tends to induce undesirable agglomeration, which reduces the effective surface area available for magnetic interaction, further limiting the magnetic response [37]. Therefore, we found that both the reduction in crystallite size and agglomeration may synergistically lower the saturation magnetization of sample T5.

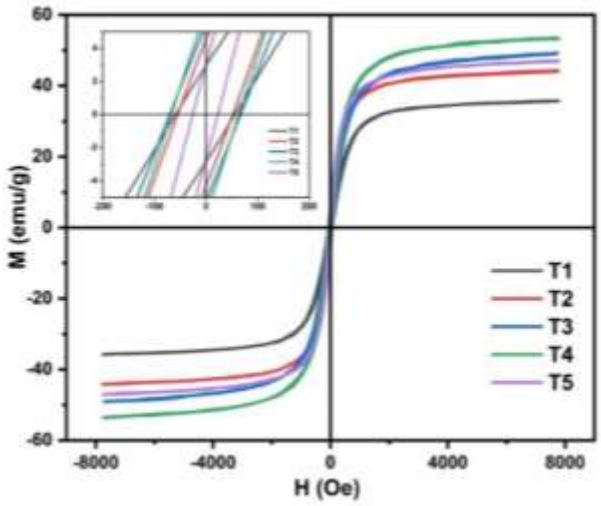

Figure 4. M-H loops of $MnFe_2O_4$ nanoparticles synthesized at different reaction times.

The magnetic properties of nanoparticles depend on many factors, including external factors such as production technique, structure, density, and internal like the magnetic moment of the material itself [32]. Furthermore, saturation magnetism (M_s) fundamentally depends on the exchange interaction between ions distributed at the tetrahedral (A-site) and octahedral (B-site) sites in the nano ferrite structure. Increasing the occupancy of Fe^{3+} or Mn^{2+} at the octahedral site increases M_s, whereas higher occupancy of metal ions at the tetrahedral site reduces M_s [20, 32]. The reaction time profoundly affects particle growth conditions and crystallinity. For shorter reaction times (T1 and T2), the reaction time is not long enough for the $MnFe_2O_4$ particles to crystallize completely, and the smaller particle size also causes a decrease in M_s. In addition, the presence of α-Fe_2O_3 impurity also contributes to the reduction in magnetism because it is a weakly magnetic phase [39]. In sample T5, the extended hydrothermal reaction resulted in the particles coalescing into larger clusters, creating structures that begin to approximate bulk behavior. The occurrence of particle agglomeration can explain the decreasing magnetism trend of sample T5 during the synthesis, which reduces the effective surface area, leading to a decrease in M_s [37, 40]. Additionally, the decrease in M_s for sample T5 compared to T4 is also influenced by the decrease in crystallite size, as previously explained.

However, these agglomerates maintain some characteristics of nanoparticles due to incomplete fusion and the presence of interface regions between aggregated particles. This partial bulk-like character explains why the M_s value (46.93 emu/g) remains significantly below that of bulk $MnFe_2O_4$,

which exhibits a much higher saturation magnetization (M_s = 82 emu/g) as reported by Aslibeiki et al. [41]. The highest remanent magnetization (M_r) and coercivity (H_c) values were observed for T4 (6.55 emu/g) and T3 (67.43 Oe), respectively. The change in M_r value follows a similar trend to that of M_s, which is expected due to their intrinsic correlation. This trend is consistent with the change in average crystallite size (calculated from XRD). Since the remanent magnetization reflects the remaining magnetism after removal of the external field, it is particularly sensitive to microstructural factors such as crystallite size and inter-grain interactions. In contrast, the coercivity (H_c) exhibits a non-linear trend due to its dependence on various factors such as crystallite size, magneto-crystalline anisotropy constant, porosity, internal stress, and crystal imperfections [5]. According to Ghahfarokhi et al., H_c tends to decrease with increasing particle size in the multi-domain regime, as larger particles may split into multiple magnetic domains, reducing the magnetization energy. Consequently, less energy is required to initiate domain wall movement, leading to a decrease in H_c. A similar behavior was observed by Majid et al. in cobalt ferrite [37], where H_c decreased due to the transition of particles into a multi-domain structure. Likewise, Ozel et al. [36] reported a reduction in H_c with prolonged reaction time in Fe_3O_4 nanoparticles, which was attributed to changes in magnetic domain structures and crystallinity.

At shorter reaction times, the presence of α-Fe_2O_3 impurities with higher concentrations affects the crystallinity and causes lattice defects. In addition, the impurity phase also increases the local magnetic anisotropy. It breaks the domain walls in the ferrite structure, which overall affects the material's magnetism, as reported by Li et al. [42]. Based on these observations, a reaction time of 4 h (sample T4) provides favorable conditions for the synthesis of $MnFe_2O_4$ nanoparticles with well-balanced magnetic properties.

The magnetic moment per ion (μ_m) was calculated using the equation [43]:

$$\mu_m = \frac{M_s \times M}{5585}$$ where M is the molecular mass of $MnFe_2O_4$.

The μ_m values calculated for the synthetic $MnFe_2O_4$ nanoparticles in our report ranged from 0.02 to 2.35 (in Tables 2 and 3) compared to the empirical value of 2.22 reported by Nguyen et al. [43], which is perfectly appropriate. However, this value is still lower than the previously reported theoretical value of 4.

Table 2. Magnetic Parameters of $MnFe_2O_4$ nanoparticles at various reaction times

Sample	Magnetic properties			
	M_s (emu/g)	M_r (emu/g)	H_c (Oe)	μ_m
T1	35,76	2,94	56,38	1.48
T2	44,2	4,5	52,34	1.83
T3	49,25	5,37	67,43	2.03
T4	53,4	6,19	64,16	2.21
T5	46,93	2,99	23,24	1.94

The magnetic hysteresis loops of $MnFe_2O_4$ nanoparticles synthesized at various pH values are presented in Fig. 5, with the corresponding magnetic parameters including saturation magnetization (M_s), coercivity (H_c), and magnetic moment μ_m) - summarized in Table 3. All samples (except sample P1) exhibited typical ferromagnetic behavior, with the magnetic response improving as pH increased. Notably, sample P4 (pH11) demonstrated the highest saturation magnetization, reaching 56.88 emu/g.

At low pH (P1, P2), the samples exhibited poor magnetic performance due to the influence of α-Fe_2O_3 impurity phase in the previously confirmed XRD results. Sample P1 had an extremely low M_s of 0.44 emu/g, remanence of magnetism (M_r) of 0.12 emu/g, and μ_m of 0.01. The impurity phase is dominant, causing a magnetically inert layer on the surface of nanoparticles in sample P1, as Nitika et al. [44] reported, reflecting incomplete phase formation and poor crystallinity due to the Fe_2O_3 oxide layer inhibiting grain growth. As the pH increases, the magnetic properties also increase sharply, which is explained by the better crystallinity that shows a clear improvement in the magnetic properties.

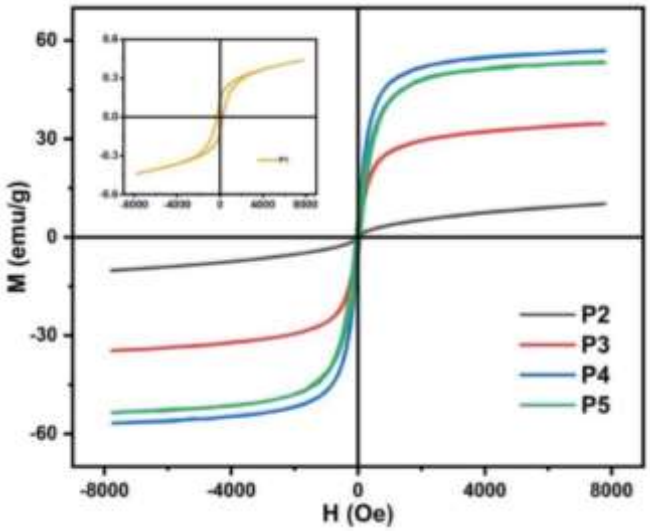

Figure 5. M-H loops of $MnFe_2O_4$ nanoparticles synthesized at different pH values.

Sample P4, synthesized at pH11, shows the highest magnetic properties among all the samples synthesized in this work, with an M_s value of 56.88 emu/g and a magnetic moment of 2.35 μ_m, a low coercivity (H_c) of 21.47 Oe. It can be seen that the optimization of pH value during synthesis is an important factor in achieving good magnetic properties of manganese ferrite nanoparticles. As evidenced by the high saturation magnetization and the greatly reduced H_c over all the investigated samples with the reaction time discussed earlier was without controlling the pH value.

Table 3. Magnetic Parameters of $MnFe_2O_4$ nanoparticles at various pH values

Sample	Magnetic properties			
	M_s (emu/g)	M_r (emu/g)	H_c (Oe)	μ_m
P1	0,44	0,12	270,95	0.02
P2	10,19	0,11	7,16	0.42
P3	34,63	1,91	21,83	1.43
P4	56,88	3,48	21,47	2.35
P5	53,4	6,19	64,16	2.21

However, at pH13 (P5), while M_s remains high at 53.4 emu/g, a slight decrease compared to P4 is observed, along with a significant increase in coercivity (H_c = 64.16 Oe). The increase in coercivity (H_c) from P4 (pH11) to P5 (pH13) may be due to the interaction between grain size and surface effect [45]. When the grain size approaches the critical single-domain size, the coercivity is mainly decided by the displacement of magnetic domains [45,46]. In this study, the increase in the average crystallite size from

10.8 nm (P4) to 24.3 nm (P5) is likely to approach the single-domain threshold, estimated to be approximately 30 nm, as reported by Kumar et al. [47]. Consequently, the energy required to rotate the magnetic domains also increases, leading to the observed rise in H_c.

In addition, high pH promotes faster precipitation, growth, and crystallization of grains. At high pH during synthesis, grain growth and crystallinity are significantly promoted. However, ions such as OH^- remaining at the particle interfaces may form heterogeneous layers around the nanoparticles. Although these ions are partly removed during washing with DI water, this process inadvertently introduces surface defects. These defects act as pinning centers, hindering the motion of domain walls and increasing magnetic anisotropy, leading to higher H_c. This behavior aligns with observations previously reported by R.N. Bhowmik [48].

Overall, the magnetic properties of $MnFe_2O_4$ are highly dependent on the synthesis pH. The optimal magnetic performance is achieved at pH11 (P4), where the combination of high M_s, low H_c, and minimal impurities makes the sample suitable for applications requiring soft magnetic behavior. These results highlight the critical role of pH in controlling the structural and magnetic characteristics of $MnFe_2O_4$ synthesized via the hydrothermal method.

Table 4. Magnetic Parameters of $MnFe_2O_4$ nanoparticles annealed at different temperatures

Sample	Magnetic properties		
	M_s (emu/g)	M_r (emu/g)	H_c (Oe)
As-prepared	56,88	3,48	21,47
200 °C	30,5	3	68
400 °C	18,8	2,5	47
600 °C	12,5	3,67	190
800 °C	0,16	0,019	314

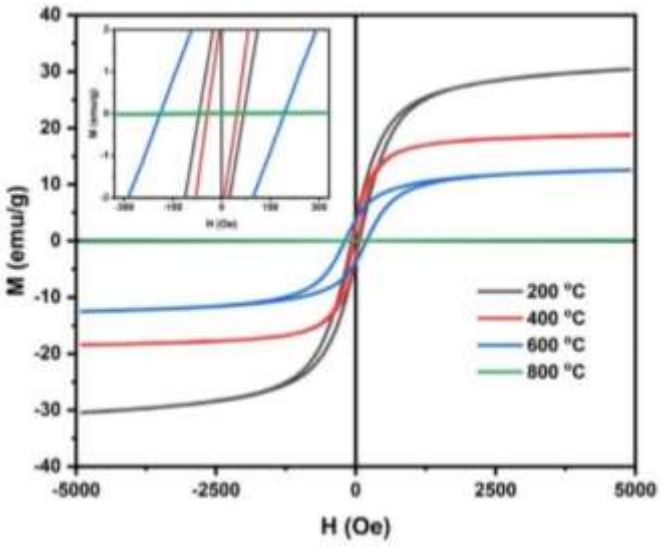

Figure 6. M-H loops of $MnFe_2O_4$ nanoparticles annealed at different temperatures.

To investigate the effect of annealing temperature on the magnetic properties of fabricated sample, we choose the P4 sample with highest magnetization for this study. Figure 6 presents the M-H loops of

$MnFe_2O_4$ nanoparticles annealed at various temperatures, with corresponding magnetic properties shown in Table 4. The annealing temperature strongly influences the saturation magnetization M_s, coercivity H_c, and remanence M_r, highlighting the impact of structural and phase evolution on magnetic behavior.

The saturation magnetization (M_s) gradually decreased from 30.5 emu/g at 200 °C to 12.5 emu/g at 600 °C and became negligible at 800 °C. This can be explained by the fact that the temperature causes the $MnFe_2O_4$ nanoparticles to decompose into component oxides such as Fe_2O_3, Mn_2O_3, and possibly FeO. These are all non-magnetic oxides, and they form dead layers on the surface of the nanoparticles, leading to a spin canting effect, thereby reducing the saturation magnetization M_s [44, 49].

The coercivity (H_c) shows a non-monotonous behavior, peaking at 600°C with a value of 190 Oe. This increase was due to the enhanced anisotropy caused by the coexistence of multiple magnetic phases, mostly nonmagnetic secondary phases. At higher temperatures, the transition from the ferrimagnetic spinel structure to the antiferromagnetic phase dominates, as seen in the linear M-H response at 800°C. These observations are consistent with the trend reported by Bhandare, where annealing leads to oxidation of Mn^{2+} to Mn^{3+}, partial decomposition of $MnFe_2O_4$ to α-Mn_2O_3 and α-Fe_2O_3, and a decrease in magnetization due to the formation of non-magnetic oxides [50].

4. Conclusions

$MnFe_2O_4$ nanoparticles were successfully synthesized via the hydrothermal method, with reaction time and pH systematically affecting their structural and magnetic properties. XRD confirmed a cubic spinel structure, with optimal crystallinity at pH11, for 4 h. Lower pH and shorter times led to α-Fe_2O_3 impurities. Fe-SEM images revealed like-spherical nanoparticles with sizes ranging from 15 to 60 nm. While the optimally dispersed regions exhibited fairly uniform particles around 25 nm in diameter, consistent with the XRD-derived crystallite size, the overall average particle size across the sample, including agglomerated areas, was approximately 40 nm. Magnetic measurements indicated soft ferromagnetism, with the best sample (pH11, for 4 h) achieving 56.88 emu/g saturation magnetization and 21.47 Oe coercivity. Crystallinity and phase purity significantly influenced magnetic properties, while excessive reaction times and extreme pH reduced performance. Annealing above 600 °C further decreased magnetism, aligning with prior studies. These findings highlight the role of pH and reaction time in tailoring $MnFe_2O_4$ nanoparticles for magnetic applications.

References

[1] K. K. Kefeni, B. B. Mamba, Photocatalytic Application of Spinel Ferrite Nanoparticles and Nanocomposites in Wastewater Treatment: Review, Sustainable Materials and Technologies, Vol. 23, 2020, pp. e00140 1-18, https://doi.org/10.1016/j.susmat.2019.e00140.

[2] S. J. Salih, W. M. Mahmood, Review on Magnetic Spinel Ferrite (MFe_2O_4) Nanoparticles: From Synthesis to Application, Heliyon, Vol. 9, Iss. 6, 2023, pp. e16601 1-25, https://doi.org/10.1016/j.heliyon.2023.e16601.

[3] N. Akhlaghi, G. N. Darzi, Manganese Ferrite ($MnFe_2O_4$) Nanoparticles: From Synthesis to Application - A Review, Journal of Industrial and Engineering Chemistry, Vol. 103, 2021, pp. 292-304, https://doi.org/10.1016/j.jiec.2021.07.043.

[4] E. M. Materón, C. M. Miyazaki, O. Carr, N. Joshi, P. H. S. Picciani, C. J. Dalmaschio, F. Davis, F. M. Shimizu, Magnetic Nanoparticles in Biomedical Applications: A Review, Applied Surface Science Advances, Vol. 6, 2021, pp. 100163 1-17, https://doi.org/10.1016/j.apsadv.2021.100163.

[5] S. E. M. Ghahfarokhi, E. M. Shobegar, Influence of pH on the Structural, Magnetic and Optical Properties of $SrFe_2O_4$ Nanoparticles, Journal of Materials Research and Technology, Vol. 9, Iss. 6, 2020, pp. 12177–12186, https://doi.org/10.1016/j.jmrt.2020.08.063.

[6] T. V. Sagar, T. S. Rao, K. C. B. Naidu, Effect of Calcination Temperature on Optical, Magnetic and Dielectric Properties of Sol-Gel Synthesized Ni0.2Mg0.8-xZnxFe2O4 (x = 0.0–0.8), Ceramics International, Vol. 46, Iss. 8, 2020, pp. 11515-11529, https://doi.org/10.1016/j.ceramint.2020.01.178.

[7] N. Boda, G. Boda, K. C. B. Naidu, M. Srinivas, K. M. Batoo, D. Ravinder, A. P. Reddy, Effect of Rare Earth Elements on Low Temperature Magnetic Properties of Ni and Co-Ferrite Nanoparticles, Journal of Magnetism and Magnetic Materials, Vol. 473, 2019, pp. 228-235, https://doi.org/10.1016/j.jmmm.2018.10.023.

[8] A. B. Nawale, N. S. Kanhe, K. R. Patil, S. V. Bhoraskar, V. L. Mathe, A. K. Das, Magnetic Properties of Thermal Plasma Synthesized Nanocrystalline Nickel Ferrite ($NiFe_2O_4$), Journal of Alloys and Compounds, Vol. 509, Iss. 12, 2011, pp. 4404-4413, https://doi.org/10.1016/j.jallcom.2011.01.057.

[9] Z. Zhang, Y. Wang, Q. Tan, Z. Zhong, F. Su, Facile Solvothermal Synthesis of Mesoporous Manganese Ferrite ($MnFe_2O_4$) Microspheres as Anode Materials for Lithium-Ion Batteries, Journal of Colloid and Interface Science, Vol. 398, 2013, pp. 185-192, https://doi.org/10.1016/j.jcis.2013.01.067.

[10] D. H. K. Reddy, Y. S. Yun, Spinel Ferrite Magnetic Adsorbents: Alternative Future Materials for Water Purification?, Coordination Chemistry Reviews, Vol. 315, 2016, pp. 90-111, https://doi.org/10.1016/j.ccr.2016.01.012.

[11] K. R. S. Lievanos, J. L. Stair, K. E. Knowles, Cation Distribution in Spinel Ferrite Nanocrystals: Characterization, Impact on their Physical Properties, and Opportunities for Synthetic Control, Inorganic Chemistry, Vol. 60, Iss. 7, 2021, pp. 4291-4305, https://doi.org/10.1021/acs.inorgchem.1c00040.

[12] K. Praveena, H. W. Chen, H. L. Liu, K. Sadhana, S. R. Murthy, Enhanced Magnetic Domain Relaxation Frequency and Low Power Losses in Zn^{2+} Substituted Manganese Ferrites Potential for High Frequency Applications, Journal of Magnetism and Magnetic Materials, Vol. 420, 2016, pp. 129-142, https://doi.org/10.1016/j.jmmm.2016.07.011.

[13] K. Praveena, K. Sadhana, S. Bharadwaj, S. R. Murthy, Development of Nanocrystalline Mn-Zn Ferrites for High Frequency Transformer Applications, Journal of Magnetism and Magnetic Materials, Vol. 321, Iss. 16, 2009, pp. 2433-2437, https://doi.org/10.1016/j.jmmm.2009.02.138.

[14] K. Praveena, G. V. J. Gowda, A. E. Denglawey, V. Jagadeesha Angadi, Manganese Ferrite-Polyaniline Nanocomposites for Microwave Absorbers in X Band, Journal of Materials Science: Materials in Electronics, Vol. 33, Iss. 8, 2022, pp. 5678-5685, https://doi.org/10.1007/s10854-022-07753-5.

[15] A. Doaga, A. M. Cojocariu, W. Amin, F. Heib, P. Bender, R. Hempelmann, O. F. Caltun, Synthesis and Characterizations of Manganese Ferrites for Hyperthermia Applications, Materials Chemistry and Physics, Vol. 143, Iss. 1, 2013, pp. 305-310, https://doi.org/10.1016/j.matchemphys.2013.08.066.

[16] C. R. Kalaiselvan, S. S. Laha, S. B. Somvanshi, T. A. Tabish, N. D. Thorat, N. K. Sahu, Manganese Ferrite ($MnFe_2O_4$) Nanostructures for Cancer Theranostics, Coordination Chemistry Reviews, Vol. 473, 2022, pp. 214809 1-32, https://doi.org/10.1016/j.ccr.2022.214809.

[17] K. Islam, M. Haque, A. Kumar, A. Hoq, F. Hyder, S. M. Hoque, Manganese Ferrite Nanoparticles (MnFe2O4): Size Dependence for Hyperthermia and Negative/Positive Contrast Enhancement in MRI, Nanomaterials, Vol. 10, Iss. 11, 2020, pp. 1-23, https://doi.org/10.3390/nano10112297.

[18] Z. Szotek, W. M. Temmerman, D. Ködderitzsch, A. Svane, L. Petit, H. Winter, Electronic Structures of Normal and Inverse Spinel Ferrites from First Principles, Physical Review B - Condensed Matter and Materials Physics, Vol. 74, Iss. 17, 2006, pp. 1-12, https://doi.org/10.1103/PhysRevB.74.174431.

[19] K. Vamvakidis, M. Katsikini, D. Sakellari, E. C. Paloura, O. Kalogirou, C. D. Samara, Reducing the Inversion Degree of $MnFe_2O_4$ Nanoparticles Through Synthesis to Enhance Magnetization: Evaluation of Their ^{1}H NMR Relaxation and Heating Efficiency, Dalton Transactions, Vol. 43, Iss. 33, 2014, pp. 12754-12765, https://doi.org/10.1039/c4dt00162a.

[20] M. M. Baig, M. A. Yousuf, P. O. Agboola, M. A. Khan, I. Shakir, M. F. Warsi, Optimization of Different Wet Chemical Routes and Phase Evolution Studies of $MnFe_2O4$ Nanoparticles, Ceramics International, Vol. 45, Iss. 10, 2019, pp. 12682–12690, https://doi.org/10.1016/j.ceramint.2019.03.114.

[21] A. Scano, G. Ennas, F. Frongia, A. L. Barbera, M. A. L. Quintela, G. Marongiu, G. Paschina, D. Peddis, M. Pilloni, C. V. Vázquez, Mn-ferrite Nanoparticles via Reverse Microemulsions: Synthesis and Characterization, Journal of Nanoparticle Research, Vol. 13, Iss. 7, 2011, pp. 3063-3073, https://doi.org/10.1007/s11051-010-0205-y.

[22] Y. K. Li, L. Cheng, X. D. Zhang, X. Guo, Hierarchically-structured $MnFe_2O_4$ Nanospheres for Highly Sensitive Detection of NO_2, Solid State Ionics, Vol. 336, 2019, pp. 102-109, https://doi.org/10.1016/j.ssi.2019.03.016.

[23] B. M. Asiabar, M. A. Karimi, H. Tavallali, M. R. Nasrabadi, Application of $MnFe_2O_4$ and AuNPs Modified CPE as A Sensitive Flunitrazepam Electrochemical Sensor, Microchemical Journal, Vol. 161, 2021, pp. 105745 1-26, https://doi.org/10.1016/j.microc.2020.105745.

[24] R. Asadi, H. Abdollahi, M. Gharabaghi, Z. Boroumand, Effective Removal of Zn (II) Ions From Aqueous Solution by the Magnetic Mn Fe_2O_4 and $CoFe_2O_4$ Spinel Ferrite Nanoparticles with Focuses on Synthesis, Characterization, Adsorption, and Desorption, Advanced Powder Technology, Vol. 31, Iss. 4, 2020, pp. 1480-1489, https://doi.org/10.1016/j.apt.2020.01.028.

[25] S. R. Sabale, Studies on Catalytic Activity of $MnFe_2O_4$ and $CoFe_2O_4$MNPsas Mediators in Hemoglobin Based Biosensor, Materials Today: Proceedings, International Conference on Materials and Environmental Science (ICMES 2018), Vol. 23, Part 2, 2020, pp. 139-146, https://doi.org/10.1016/j.matpr.2020.02.011.

[26] N. Sezgin, A. Yalçın, Y. Köseoğlu, Mn Fe_2O_4 Nano Spinels as Potential Sorbent for Adsorption of Chromium from Industrial Wastewater, Desalination and Water Treatment, Vol. 57, Iss. 35, 2016, pp. 16495-16506, https://doi.org/10.1080/19443994.2015.1088808.

[27] J. M. Kwon, J. H. Kim, S. H. Kang, C. J. Choi, J. A. Rajesh, K. S. Ahn, Facile Hydrothermal Synthesis of Cubic Spinel AB_2O_4 Type $MnFe_2O_4$ Nanocrystallites and Their Electrochemical Performance, Applied Surface Science, Vol. 413, 2017, pp. 83-91, https://doi.org/10.1016/j.apsusc.2017.04.022.

[28] H. Tombuloglu, G. Tombuloglu, Y. Slimani, I. Ercan, H. Sozeri, A. Baykal, Impact of Manganese Ferrite ($MnFe_2O_4$) Nanoparticles on Growth and Magnetic Character of Carley (Hordeum vulgare L.), Environmental Pollution, Vol. 243, Part B, 2018, pp. 872-881, https://doi.org/10.1016/j.envpol.2018.08.096.

[29] W. Zhang, X. Hou, Z. Lin, L. Yao, X. Wang, Y. Gao, S. Hu, Hollow Microspheres and Nanoparticles Mn Fe_2O_4 as Superior Anode Materials for Lithium Ion Batteries, Journal of Materials Science: Materials in Electronics, Vol. 26, Iss. 12, 2015, pp. 9535–9545, https://doi.org/10.1007/s10854-015-3616-9.

[30] L. Shao, Z. Ren, G. Zhang, L. Chen, Facile Synthesis, Characterization of A $MnFe_2O_4$/Activated Carbon Magnetic Composite and Its Effectiveness in Tetracycline Removal, Materials Chemistry and Physics, Vol. 135, Iss. 1, 2012, pp. 16-24, https://doi.org/10.1016/j.matchemphys.2012.03.035.

[31] B. D. Cullity & S.R. Stock, Elements of X-Ray Diffraction, 3rd Ed., Prentice-Hall Inc., ISBN 0-201-61091-4, 2001, pp. 96-102,

[32] Z. Jabeen, A. Dawood, M. Alomar, S. N. Khan, I. Ali, M. Asif, W. Abbas, M. Sultan Irshad, M. Ahmad, Hydrothermal Synthesis of Nickel Substituted Magnesium Ferrites ($NixMg1\text{-}xFe_2O_4$) and Insight into The Detailed Structural, Magnetic and Electrochemical Properties, Surfaces and Interfaces, Vol. 40, 2023, pp. 103130 1-9, https://doi.org/10.1016/j.surfin.2023.103130.

[33] P. Zhang, Y. Shu, Y. Zhong, L. Yang, X. Yang, CoZnFeO4 Prepared by Waste Ferrous Sulfate as Iron Source: Synthesis, Characterization and Photocatalytic Degradation of Methylene Blue, Journal of Materials Science: Materials in Electronics, Vol. 32, Iss. 16, 2021, pp. 20985–21011, https://doi.org/10.1007/s10854-021-06562-6.

[34] A. Solunke, V. K. Barote, B. Sonawane, S. E. Shirsath, R. H. Kadam, V. S. Shinde, Sol-gel Synthesis of Fe-rich Cobalt Ferrite Nanoparticles and Influence of pH Concentration, Materials Today: Proceedings, Vol. 92, Part 2, 2023, pp. 1225–1230, https://doi.org/10.1016/j.matpr.2023.05.327.

[35] O. Karaagac, H. Köçkar, The Effects of Temperature and Reaction Time on The Formation of Manganese Ferrite Nanoparticles Synthesized by Hydrothermal Method, Journal of Materials Science: Materials in Electronics, Vol. 31, Iss. 3, 2020, pp. 2567–2574, https://doi.org/10.1007/s10854-019-02795-8.

[36] F. Ozel, H. Kockar, O. Karaagac, Growth of Iron Oxide Nanoparticles by Hydrothermal Process: Effect of Reaction Parameters on the Nanoparticle Size, Journal of Superconductivity and Novel Magnetism, Vol. 28, Iss. 3, 2015, pp. 823-829, https://doi.org/10.1007/s10948-014-2707-9.

[37] F. Majid, A. Nazir, S. Ata, I. Bibi, H. S. Mehmood, A. Malik, A. Ali, M. Iqbal, Effect of Hydrothermal Reaction Time on Electrical, Structural and Magnetic Properties of Cobalt Ferrite, Zeitschrift fur Physikalische Chemie, Vol. 234, Iss. 2, 2020, pp. 323–353, https://doi.org/10.1515/zpch-2019-1423.

[38] S. Upadhyay, K. Parekh, B. Pandey, Influence of Crystallite Size on The Magnetic Properties of Fe_3O_4 Nanoparticles, Journal of Alloys and Compounds, Vol. 678, 2016, pp. 478-485, https://doi.org/10.1016/j.jallcom.2016.03.279.

[39] J. Sahadevan, R. Sojiya, N. Padmanathan, K. Kulathuraan, M. G. Shalini, P. Sivaprakash, Magnetic Property of Fe_2O_3 and Fe_3O_4 Nanoparticle Prepared by Solvothermal Process, Materials Today: Proceedings, International Conference on Novel Engineering Materials for Biomedical, Energy, Environment, Sensing, and Other Applications, Vol. 58, Part 3, 2022, pp. 895-897,https://doi.org/10.1016/j.matpr.2021.11.420.

[40] Y. Ge, Y. Zhang, J. Xia, M. Ma, S. He, F. Nie, N. Gu, Effect of Surface Charge and Agglomerate Degree of Magnetic Iron Oxide Nanoparticles on KB Cellular Uptake in Vitro, Colloids and Surfaces B: Biointerfaces, Vol. 73, Iss. 2, 2009, pp. 294-301, https://doi.org/10.1016/j.colsurfb.2009.05.031.

[41] B. Aslibeiki, P. Kameli, M. H. Ehsani, Mn Fe_2O_4 Bulk, Nanoparticles and Film: A Comparative Study of Structural and Magnetic Properties, Ceramics International, Vol. 42, Iss. 11, 2016, pp. 12789–12795, https://doi.org/10.1016/j.ceramint.2016.05.041.

[42] L. Z. Li, Z. Yu, Z. W. Lan, K. Sun, R. Di Guo, Effects of Annealing Temperature on The Structure and Static Magnetic Properties of NiZnCo Ferrite Thin Films, Journal of Magnetism and Magnetic Materials, Vol. 368, 2014, pp. 8–11, https://doi.org/10.1016/j.jmmm.2014.05.005.

[43] L. H. Nguyen, L. T. Tam, N. H. Nam, D. K. Tung, N. X. Truong, D. V. Tuan, N. V. Quynh, N. L. M. Tri, P.T. Phong, P. H. Nam, Evaluation of Structural, Optical, and Magnetic Properties of Gd Doped $MnFe_2O_4$ Nanoparticles, Ceramics International, Vol. 49, Iss. 24, 2023, pp. 40981–40989, https://doi.org/10.1016/j.ceramint.2023.10.092.

[44] Nitika, A. Rana, V. Kumar, Influence of Temperature on Structural, Magnetic and Thermal Properties of Superparamagnetic $MnFe_2O_4$ Nanoparticles, Materials Today: Proceedings, Second International Conference on Aspects of Materials Science and Engineering (ICAMSE 2021), Vol. 45, Part 6, 2021, pp. 4774–4776, https://doi.org/10.1016/j.matpr.2021.01.209.

[45] I. Anila, M. J. Mathew, Influence of pH on Structural and Magnetic Properties of Nanocrystalline Cobalt Ferrites Synthesized by Sol-gel Method, AIP Conference Proceedings, Vol. 2162, No. 1, 2019, pp. 1-7, https://doi.org/10.1063/1.5130287.

[46] A. Pradeep, P. Priyadharsini, G. Chandrasekaran, Sol-gel Route of Synthesis of Nanoparticles of $MgFe_2O_4$ and XRD, FTIR and VSM Study, Journal of Magnetism and Magnetic Materials, Vol. 320, Iss. 21, 2008, pp. 2774–2779, https://doi.org/10.1016/j.jmmm.2008.06.012.

[47] P. Kumar, S. Pathak, K. Jain, A. Singh, Kuldeep, G. A. Basheed, R. P. Pant, Low-Temperature Large-Scale Hydrothermal Synthesis of Optically Active PEG-200 Capped Single Domain $MnFe_2O_4$ Nanoparticles, Journal of Alloys and Compounds, Vol. 904, 2022, pp. 163992 1-8, https://doi.org/10.1016/j.jallcom.2022.163992.

[48] R. N. Bhowmik, Role of Interfacial Disorder on Room Temperature Ferromagnetism and Giant Dielectric Constant in Nano-sized Co1.5Fe1.5O4 Ferrite Grains, Materials Research Bulletin, Vol. 50, No. 1, 2014, pp. 476–482, https://doi.org/10.1016/j.materresbull.2013.11.017.

[49] M. Zhen, X. Wu, B. Zou, Y. Wang, Magnetic Properties of Nanosized MnFe2O4 Particles, Journal of Magnetism and Magnetic Materials, Vol. 183, Iss. 1-2, 1998, pp. 152–156, https://doi.org/10.1016/S0304-8853(97)01057-3.

[50] S. V. Bhandare, R. Kumar, A. V. Anupama, H. K. Choudhary, V. M. Jali, B. Sahoo, Annealing Temperature Dependent Structural and Magnetic Properties of $MnFe_2O_4$ Nanoparticles Grown by Sol-gel Auto-combustion Method, Journal of Magnetism and Magnetic Materials, Vol. 433, 2017, pp. 29-34, https://doi.org/10.1016/j.jmmm.2017.02.040.